

Towards Attenuation Imaging with Computed Ultrasound Tomography in Echo Mode (CUTE)

Naiara Korta Martiartu
Institute of Applied Physics
University of Bern
Bern, Switzerland
naiara.korta@unibe.ch

Parisa Salemi Yolgunlu
Institute of Applied Physics
University of Bern
Bern, Switzerland
parisa.salemi@unibe.ch

Patrick Stähli
Insel Data Science Center
Bern University Hospital
Bern, Switzerland

Martin Frenz
Institute of Applied Physics
University of Bern
Bern, Switzerland
martin.frenz@unibe.ch

Michael Jaeger
Institute of Applied Physics
University of Bern
Bern, Switzerland
michael.jaeger@unibe.ch

Abstract—This work presents a novel attenuation imaging technique for pulse-echo ultrasound systems. In contrast to state-of-the-art techniques, we formulate the reconstruction in two dimensions relying on tissue insonifications with different steering angles. By beamforming backscattered echoes recorded by the transducer, we measure at each location the changes in the amplitudes of detected echoes with different transmissions and relate them to local tissue attenuation. This relationship assumes ultrasound waves propagate in straight paths; thus, we linearize the forward problem to provide suitable time-to-solutions for clinical practice. The presented technique is the natural extension of computed tomography in echo mode (CUTE), initially developed for tissue speed-of-sound quantification. The performance of our method is demonstrated in numerical examples with data computed using the k-Wave numerical solver for wave-propagation simulations. These examples consider tissue-mimicking media with varying heterogeneity in attenuation and echogenicity. The results show that our method can provide images with promising spatial and contrast resolution, as well as attenuation estimates independent of tissue echogenicity. This work represents a necessary first step towards multi-modal CUTE imaging of speed of sound and attenuation in tissue.

Index Terms—ultrasound attenuation, pulse-echo ultrasound, tissue characterization, tomography, diffuse scattering

I. INTRODUCTION

The attenuation (ATT) of ultrasound (US) waves varies with tissue absorption and scattering properties and can therefore be used to identify different tissue types or pathologies. For instance, the controlled attenuation parameter (CAP), estimating the average ATT undergone by ultrasound waves in their propagation, has become the standard tool to diagnose hepatic steatosis noninvasively [1], [2]. Despite its good diagnostic performance, CAP has two main limitations: (i) it is exclusively designed for liver assessment, thereby having a limited application range, and (ii) it provides a single ATT value for a

predefined region of interest and cannot thus characterize the inherent tissue heterogeneity.

Imaging modalities quantifying the spatial distribution of tissue ATT can overcome these limitations. In the past years, several techniques have been suggested to image this property. They include, for instance, spectral-log difference approaches [3], [4], which estimate ATT from depth-dependent spectral amplitude variations of backscattered echoes, and spectral-shift methods, which rely on the frequency downshift of the spectrum caused by ATT [5], [6]. The vast majority of these methods use simplified one-dimensional formulations that consider US waves propagating only in the axial direction. Such simplifications, however, limit the spatial resolution of reconstructed images due to poor physical constraints [7]. As shown by state-of-the-art pulse-echo speed-of-sound (SoS) imaging techniques, we can improve this aspect by interrogating tissue properties with waves propagating along multiple directions. This is the approach used in computed tomography in echo mode (CUTE), which tracks echo phase shifts caused by SoS heterogeneities when probing tissue at different angles [8]–[10]. CUTE has demonstrated unprecedented spatial and contrast resolution in tissue-mimicking phantoms [11] and is currently undergoing clinical evaluation [12].

This work presents an extension of CUTE to quantify the spatial distribution of US ATT in tissue. This new technique relies on measurements of echo-amplitude variations at each location when they are detected using plane-wave transmissions with different steering angles. In the following, we briefly introduce the theoretical relationship between local echo-amplitude variations and US ATT in tissue. We then explain the approach used to measure these amplitude variations and finally present numerical examples showing the performance of the proposed technique.

This research has been funded by the Swiss National Science Foundation under project no. 205320_179038. N. K. M. thanks the support of the University of Bern through the UniBe Initiator Grant.

II. FORWARD MODELING

The derivations presented herein are formulated in the temporal frequency domain, where ω refers to the angular frequency. Assume we emit a plane wave with amplitude $A(\omega)$ propagating in direction \mathbf{k} to insonify a medium defined in the spatial domain Ω with scattering coefficient $\chi(\mathbf{x})$, where $\mathbf{x} \in \Omega$. If multiple-scattering is neglected, we can express the backscattered wavefield $p(\mathbf{x}_r, \mathbf{k})$ recorded at location \mathbf{x}_r in terms of the Green's function G as

$$p(\mathbf{x}_r, \mathbf{k}) = \int_{\Omega} \chi(\mathbf{x}) A(\omega) \exp(j\mathbf{k} \cdot \mathbf{x}) G(\mathbf{x}_r, \mathbf{x}, \omega) d\mathbf{x}. \quad (1)$$

In lossy media, \mathbf{k} is complex, i.e., $\mathbf{k} = \mathbf{k}^r + j\mathbf{k}^i$, where $k^i = \alpha$ describes the acoustic absorption of the medium contributing to the ATT of US waves [13]. Here, we make no distinction between ATT and absorption. In tissue, ATT obeys the frequency power law $\alpha = \alpha_0 \omega^y$, where α_0 is the ATT coefficient, and y is the power law exponent typically ranging from 1 to 2 [14].

Let us now define the ensemble-averaged cross-correlation between two signals recorded at the same location and corresponding to different plane-wave transmissions, i.e., $C(\mathbf{k}_1, \mathbf{k}_2) := \langle p^*(\mathbf{x}_r; \mathbf{k}_2) p(\mathbf{x}_r; \mathbf{k}_1) \rangle$. We consider tissue as a diffuse scattering medium, meaning that scatterers are spatially uncorrelated and satisfy $\langle \chi^*(\mathbf{x}_2) \chi(\mathbf{x}_1) \rangle = \chi(\omega) \delta(\mathbf{x}_1 - \mathbf{x}_2)$ [15]. In this case, it is possible to find that $C(\mathbf{k}_1, \mathbf{k}_2)$ reduces to

$$C(\mathbf{k}_1, \mathbf{k}_2) \propto \exp(j(\mathbf{k}_1^r - \mathbf{k}_2^r) \cdot \mathbf{x}_0) \exp(-(\mathbf{k}_1^i + \mathbf{k}_2^i) \cdot \mathbf{x}_0) \quad (2)$$

for signal contributions arriving from the vicinity of an arbitrary scatterer located at \mathbf{x}_0 . Omitted terms are related to the spherical divergence, scattering amplitude $\chi(\omega)$, and amplitude of plane waves. We can make their contribution negligible by taking small angular differences between \mathbf{k}_1 and \mathbf{k}_2 and normalizing (2) with the autocorrelation. Then, we extract ATT information by taking the log-amplitude as

$$(\mathbf{k}_2^i - \mathbf{k}_1^i) \cdot \mathbf{x}_0 \approx -\log \left| \frac{C(\mathbf{k}_1, \mathbf{k}_2)}{C(\mathbf{k}_1, \mathbf{k}_1)} \right|. \quad (3)$$

Assuming waves propagating as straight rays, the forward problem in (3) becomes linear and can generally be expressed as

$$\mathbf{d} = \mathbf{F}\mathbf{m}, \quad (4)$$

where \mathbf{d} is a vector containing observed log-amplitudes at each tissue location, \mathbf{m} refers to ATT values α at each location of the reconstruction grid, and \mathbf{F} is the forward operator whose rows contain discretized ray paths in directions $(\hat{\mathbf{k}}_2^i - \hat{\mathbf{k}}_1^i) \cdot \mathbf{x}_0$ for each observational point \mathbf{x}_0 .

III. INVERSE PROBLEM

We reconstruct the spatial distribution of tissue ATT by formulating the inversion as a regularized least-squares minimization problem, where the solution is given by [16]

$$\mathbf{m}_{\text{est}} = (\mathbf{F}^T \mathbf{F} + \lambda \mathbf{L}^T \mathbf{L})^{-1} \mathbf{F}^T \mathbf{d}. \quad (5)$$

Here, \mathbf{L} is the first-order finite-difference operator penalizing highly oscillating solutions (Tikhonov regularization), and λ denotes the regularization parameter, which we optimize using the L-curve method [17]. Equation 5 assumes normally distributed noise, equal for all observations [18].

IV. NUMERICAL SIMULATIONS

We use the k-Wave open-source toolbox [19] for numerical simulations of two-dimensional US wave propagation in lossy media, with simulation parameters summarized in Table I. All tissue-mimicking phantoms in our examples have constant density and SoS, with values of 1000 kg/m² and 1480 m/s, respectively, as well as constant power-law exponent $y = 1.9$ to minimize SoS dispersion effects [14]. The speckle scattering characteristics of tissues are simulated by introducing normally distributed (mean: 0; standard deviation: 0.008) random perturbations of the acoustic impedance at each grid point of the simulation mesh. Our examples consider five different phantoms, all consisting of a homogeneous background with $\alpha_0 = 0.5$ dB/cm/MHz^{1.9} and a circular inclusion located at 1.5 cm depth. Properties of the circular inclusion in each phantom are summarized in Table II.

TABLE I
SIMULATION PARAMETERS USED IN K-WAVE

| Parameter | Value |
|-----------------------|------------------------------|
| Transducer: | |
| Type | Linear |
| Number of elements | 256 |
| Pitch | 0.2 mm |
| Source signal: | |
| Type | Tone burst |
| Center frequency | 3 MHz |
| Envelope | Gaussian |
| Number of cycles | 5 |
| Transmit plane-waves: | |
| Steering angles | $-30^\circ, \dots, 30^\circ$ |
| Angular interval | 0.5° |
| Mesh: | |
| Axial resolution | 0.1 mm |
| Lateral resolution | 0.1 mm |

V. LOG-AMPLITUDE MEASUREMENTS

We measure the spatial distribution of cross-correlation log-amplitudes in (3) following a similar approach as in the old CUTE method for phase-shift tracking. We refer the reader to [8], [10] for a more detailed description and summarize here the main steps. First, we transform measured radio-frequency signals into analytic signals using the Hilbert transform and reconstruct a complex radio-frequency image per transmission using delay-and-sum beamforming with SoS value 1480 m/s. Then, we synthetically focus the images in transmission using coherent compounding to reduce clutter for angles ranging from -25° to 25° with an angular step of 2.5° . Finally, we extract the log-amplitude information by computing zero-lag complex cross-correlations between images of successive angle pairs and by normalizing them with auto-correlations.

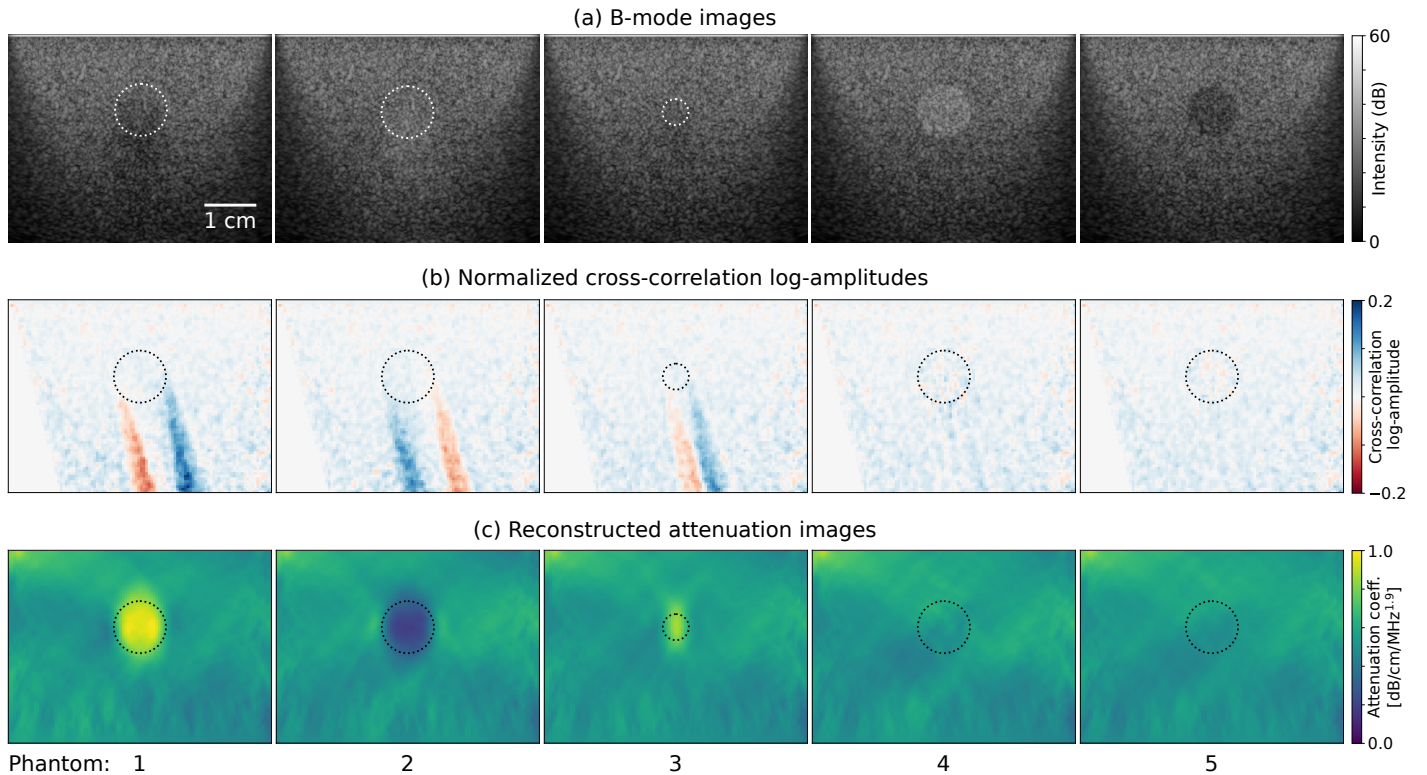


Fig. 1. Numerical results using ultrasound data computed from the k-Wave wave-propagation simulation solver. (a) B-mode images showing the spatial distribution of echo intensity for the phantoms considered in this study (Table II). (b) Example images of the spatial distribution of normalized cross-correlation log-amplitudes [see (3)] for transmissions with steering angles 15° and 17.5° . (c) Reconstructed images of the spatial distribution of attenuation coefficient. Dashed circles indicate the location and size of the circular inclusion.

TABLE II
PROPERTIES OF THE CIRCULAR INCLUSION IN EACH PHANTOM

| Property | Contrast*/Value |
|-------------------------|-------------------------------|
| Phantom 1: | |
| Attenuation coefficient | +0.5 dB/cm/MHz ^{1.9} |
| Echogenicity | 0 |
| Diameter | 1 cm |
| Phantom 2: | |
| Attenuation coefficient | -0.4 dB/cm/MHz ^{1.9} |
| Echogenicity | 0 |
| Diameter | 1 cm |
| Phantom 3: | |
| Attenuation coefficient | +0.5 dB/cm/MHz ^{1.9} |
| Echogenicity | 0 |
| Diameter | 0.5 cm |
| Phantom 4: | |
| Attenuation coefficient | 0 dB/cm/MHz ^{1.9} |
| Echogenicity | +6 dB |
| Diameter | 1 cm |
| Phantom 5: | |
| Attenuation coefficient | 0 dB/cm/MHz ^{1.9} |
| Echogenicity | -6 dB |
| Diameter | 1 cm |

*with respect to the background.

VI. NUMERICAL EXAMPLES

Numerical examples shown herein consider a rectilinear grid with a 0.5-mm mesh size in axial and lateral directions for ATT reconstructions and ensemble-averaged cross-correlations over

five realizations of the random scattering media. Moreover, we use the same regularization parameter $\lambda = 10^{-5}$ for all examples to facilitate comparisons.

In Fig. 1(a), we display the B-mode images corresponding to all phantoms considered here. We observe shadowing or enhancement artifacts when the inclusion has a positive or negative ATT contrast, respectively, and areas of different echogenicity for inclusions having random scatterers with different statistics compared to the background medium. Fig. 1(b) shows an example of observed cross-correlation log-amplitudes between beamformed images corresponding to transmission angles 15° and 17.5° . At each location, log-amplitude values are related to differences in the cumulative amplitude loss that plane waves underwent along their paths. When the ATT of the inclusion varies with respect to the background (phantoms 1-3), we observe *tails* of positive and negative log-amplitude values below the inclusion, similar to the ones observed in the echo phase shift for circular SoS heterogeneities [8]. For phantoms 4 and 5, log-amplitude measurements appear insensitive to inclusions with echogenicity contrast.

Reconstructed ATT images for each phantom are shown in Fig. 1(c). In all cases, the spatial distribution and quantitative values of ATT estimates are in excellent agreement with the true media. Importantly, these results demonstrate that our

method is robust against variations in tissue echogenicity (phantoms 4-5). Still, we can observe several artifacts in the reconstructed images: (1) Inclusions with ATT contrast appear slightly more elongated in the axial direction compared to the actual inclusion shape due to the limited angle aperture of pulse-echo systems (e.g., see phantom 3). Similarly, in the lateral direction, they show unexpectedly low or high ATT values at the edges for inclusions with positive and negative contrast, respectively. (2) The reconstructed background medium oscillates around the true value, with a standard deviation of 0.06 dB/cm/MHz^{1.9}. Probably, this is caused by the noise in log-amplitude measurements arising from clutter, side lobes, and edge waves, among others, and the limited data coverage particularly affecting the deepest regions.

VII. DISCUSSION AND CONCLUSION

In this work, we present preliminary numerical results demonstrating the potential of CUTE to quantify the spatial distribution of US ATT in tissue. Contrary to state-of-the-art ATT imaging techniques, our method uses two-dimensional physical constraints to provide images with improved spatial resolution. Specifically, we extract ATT information by measuring the changes in detected echo amplitudes when we insonify tissue using different steered plane waves. This approach does not have additional technical or computational requirements compared to the algorithm used in CUTE SoS imaging. Thus, both modalities can be easily integrated into a single framework to simultaneously provide tissue ATT and SoS images.

Our method relies on two main assumptions. Firstly, we assume that scatterers are randomly and uniformly distributed in tissue, acting as diffuse reflectors with an isotropic radiation pattern. However, tissue can also contain specular reflectors that backscatter waves in directions that depend on the transmitted plane waves. Secondly, we neglect amplitude variations caused by SoS heterogeneities resulting from geometrical focusing/defocusing, diffraction, and interference effects [20], [21]. Furthermore, such heterogeneities can also introduce aberration artifacts in beamformed images, thereby unfocusing detected echoes and affecting their amplitudes. Future work will focus on understanding the influence of these assumptions on the performance of our method using media with higher complexity.

ACKNOWLEDGMENT

The authors would like to thank Samuel Beuret for discussions about wave-propagation simulations.

REFERENCES

- [1] M. Sasso, M. Beaugrand, V. de Ledinghen, C. Douvin, P. Marcellin, R. Poupon, L. Sandrin, and V. Miette, "Controlled Attenuation Parameter (CAP): A Novel VCTE™ Guided Ultrasonic Attenuation Measurement for the Evaluation of Hepatic Steatosis: Preliminary Study and Validation in a Cohort of Patients with Chronic Liver Disease from Various Causes," *Ultrasound in Medicine & Biology*, vol. 36, no. 11, pp. 1825–1835, 2010.
- [2] S. Baumeler, W. Jochum, J. Neuweiler, I. Bergamin, and D. Semela, "Controlled attenuation parameter for the assessment of liver steatosis in comparison with liver histology: a single-centre real life experience," *Swiss medical weekly*, vol. 149, no. 1718, 2019.

- [3] A. L. Coila and R. Lavarello, "Regularized spectral log difference technique for ultrasonic attenuation imaging," *IEEE Transactions on Ultrasonics, Ferroelectrics, and Frequency Control*, vol. 65, no. 3, pp. 378–389, 2018.
- [4] Y. Labyed and T. A. Bigelow, "A theoretical comparison of attenuation measurement techniques from backscattered ultrasound echoes," *The Journal of the Acoustical Society of America*, vol. 129, no. 4, pp. 2316–2324, 2011.
- [5] D. M. Brandner, X. Cai, J. Foiret, K. W. Ferrara, and B. G. Zagar, "Estimation of Tissue Attenuation from Ultrasonic B-Mode Images—Spectral-Log-Difference and Method-of-Moments Algorithms Compared," *Sensors*, vol. 21, no. 7, 2021.
- [6] R. Kuc, "Estimating acoustic attenuation from reflected ultrasound signals: Comparison of spectral-shift and spectral-difference approaches," *IEEE Transactions on Acoustics, Speech, and Signal Processing*, vol. 32, no. 1, pp. 1–6, 1984.
- [7] N. Rawlinson and W. Spakman, "On the use of sensitivity tests in seismic tomography," *Geophysical Journal International*, vol. 205, no. 2, pp. 1221–1243, 03 2016.
- [8] M. Jaeger, G. Held, S. Peeters, S. Preisser, M. Grünig, and M. Frenz, "Computed ultrasound tomography in echo mode for imaging speed of sound using pulse-echo sonography: proof of principle," *Ultrasound in medicine and biology*, vol. 41, no. 1, pp. 235–250, 2015.
- [9] M. Jaeger, P. Stähli, N. Korta Martiartu, P. Salemi Yolgunlu, T. Frappart, C. Fraschini, and M. Frenz, "Pulse-echo speed-of-sound imaging using convex probes," 2022.
- [10] P. Stähli, M. Kuriakose, M. Frenz, and M. Jaeger, "Improved forward model for quantitative pulse-echo speed-of-sound imaging," *Ultrasonics*, p. 106168, 2020.
- [11] P. Stähli, M. Frenz, and M. Jaeger, "Bayesian Approach for a Robust Speed-of-Sound Reconstruction Using Pulse-Echo Ultrasound," *IEEE transactions on medical imaging*, vol. 40, no. 2, pp. 457–467, 2020.
- [12] P. Stähli, C. Becchetti, N. Korta Martiartu, A. Berzigotti, M. Frenz, and M. Jaeger. (2022) First-in-human diagnostic study of hepatic steatosis with computed ultrasound tomography in echo mode (CUTE).
- [13] B. E. Treeby and B. T. Cox, "Modeling power law absorption and dispersion for acoustic propagation using the fractional laplacian," *The Journal of the Acoustical Society of America*, vol. 127, no. 5, pp. 2741–2748, 2010.
- [14] T. L. Szabo, "Chapter 4 - attenuation," in *Diagnostic Ultrasound Imaging: Inside Out (Second Edition)*, 2nd ed., T. L. Szabo, Ed. Boston: Academic Press, 2014, pp. 81–119.
- [15] R. Mallart and M. Fink, "The van cittert–zernike theorem in pulse echo measurements," *The Journal of the Acoustical Society of America*, vol. 90, no. 5, pp. 2718–2727, 1991.
- [16] N. Korta Martiartu, C. Boehm, and A. Fichtner, "3-D Wave-Equation-Based Finite-Frequency Tomography for Ultrasound Computed Tomography," *IEEE Transactions on Ultrasonics, Ferroelectrics, and Frequency Control*, vol. 67, no. 7, pp. 1332–1343, 2020.
- [17] P. C. Hansen and D. P. O’Leary, "The use of the l-curve in the regularization of discrete ill-posed problems," *SIAM Journal on Scientific Computing*, vol. 14, no. 6, pp. 1487–1503, 1993.
- [18] N. Korta Martiartu, C. Boehm, V. Hapla, H. Maurer, I. J. Balic, and A. Fichtner, "Optimal experimental design for joint reflection-transmission ultrasound breast imaging: From ray- to wave-based methods," *The Journal of the Acoustical Society of America*, vol. 146, no. 2, pp. 1252–1264, 2019.
- [19] B. E. Treeby and B. T. Cox, "k-Wave: MATLAB toolbox for the simulation and reconstruction of photoacoustic wave fields," *Journal of Biomedical Optics*, vol. 15, no. 2, pp. 1 – 12, 2010.
- [20] F. A. Dahlen and A. M. Baig, "Fréchet kernels for body-wave amplitudes," *Geophysical Journal International*, vol. 150, no. 2, pp. 440–466, 08 2002.
- [21] N. Korta Martiartu, "Tomography across scales: Knowledge transfer from seismology to imaging breast tissue with ultrasound," Ph.D. dissertation, Eidgenössische Technische Hochschule, Zürich, Schweiz, Oct 2019.